Synthesis, inhibition effects and thermodynamic studies of novel substituted quinolines on the corrosion of mild steel in 1 M HCl solution

M. Rbaa[1], M. Galai[2], M. EL Faydy[1], Y. El Kacimi[2], M. Ebn Touhami[2], A. Zarrouk[3], B. Lakhrissi[1*]

[1]Laboratory of Agro-Resources, Polymers and Process Engineering, Department of Chemistry, Faculty of Science, Ibn Tofail University, PO Box 133, 14000, Kenitra, Morocco
[2]Laboratory of Materials Engineering and Environment: Application and Modeling, Faculty of Science, Ibn Tofail University, PO Box 133, 14000, Kenitra, Morocco
[3]LC2AME, Faculty of Science, First Mohammed University, PO Box 717, 60 000 Oujda, Morocco

Corresponding author: b.lakhrissi2012@gmail.com

Abstract

Two newly substituted quinoline derivatives, namely 5-((2-(4-dimethylamino)-phenyl-1H-benzo[d]imidazol-1-yl)-methyl)-quinolin-8-ol *(Q-N(CH₃)₂)* and 5-((2-(4-nitrophenyl)-1H-benzo[d]imidazol-1-yl)-methyl)-quinolin-8-ol *(Q-NO₂)* were synthesized and characterized by ^{1}H and ^{13}C NMR spectroscopy. Their inhibitory performance was studied against the corrosion of carbon steel in 1 M hydrochloric acid at 298 K. Data obtained from EIS measurements has been examined and characterized by weight loss, Tafel polarization and electrochemical impedance spectroscopy (EIS). The experimental results reveal that the studied compounds have good inhibiting effects on the corrosion for carbon steel in 1 M HCl medium. The protection efficiency increases with increasing inhibitor concentration but decrease with temperature. Polarization studies analyzed to model the corrosion inhibition process through appropriate equivalent circuit model; a constant phase element (CPE) has been used. The both inhibitors were found to obey Langmuir adsorption isotherm and Kinetic-Thermodynamic Model of El-Awady. Potentiodynamic polarization studies have shown that substituted quinolines acts as a mixed type of inhibitor's.

1. Introduction

Mild steel has been widely used as a main construction material for piping works in various industries. It has found applications in down Whole casing or tubing, flow lines and transmission or distribution pipelines in oil and gas industries [1-3]. Petroleum oil well acidization is an essential technique that is routinely used in oil and gas industries for the purpose of stimulating oil-well to ensure enhanced oil production [4, 5]. This process however endangers the life of steel gadgets as a result of acid driven corrosion. In order to prevent this undesirable reaction, corrosion inhibitors are often added to the acid solution during acidification process [6-8].
These compounds inhibit corrosion by adsorbing on metallic surface using heteroatoms (e.g. N, O, S), polar functional groups (e.g. -OH, -NH₂, -NO₂, etc.), pi-electrons and aromatic rings as adsorption centers [9-11]. Inhibitors retard metal corrosion by adsorbing on metallic surface and the process is influenced by some factors, which include molecular size of inhibitor, nature of substituents, inhibitor concentration, solution temperature and nature of test solution. [8, 9, 11]

These compounds can form either a strong coordination bond with metal atom or a passive film on the surface [12]. The corrosion inhibition of a metal may involve either physisorption or chemisorption of the inhibitor on the metal surface. Electrostatic attraction between the charged hydrophilic groups and the charged active centers on the metal surface leads to physisorption. Several authors showed that most inhibitors were adsorbed on the metal surface by displacing water molecules from the surface and forming a compact barrier film [13].

Perusal of literature reveals that many *N*-heterocyclic compounds such as pyrimidine derivatives [14], triazole derivatives [15], tetrazole derivatives [16], pyrazole derivative [17], bipyrazole derivatives [18], phenyltetrazole derivatives [7,19], pyridazine derivatives [20], benzimidazole derivatives, quinoline derivatives [21-23] to mention but a few, have been used for the corrosion inhibition of iron or steel in acidic media. The effectiveness of quinoxaline derivatives (N-heterocyclic compounds) as effective corrosion inhibitors for mild steel in sulphuric acid media has been reported [24-26].

Quinolines and their derivatives are important constituents of pharmacologically active synthetic compounds [27], including biological activities such as DNA binding capabilities [28], antitumor [29] and DNA- intercalating carrier [30]. Several 8-aminoquinoline compounds, for instance Primaquine, have been applied as chemotherapeutics for treatment of malaria disease [31]. Recently, the first quinoline-based structure (GS-9137) with very strong antiretroviral activity for HIV treatment has been synthesized [32]. Although some quinoline derivatives has been reported as corrosion inhibitors for steel in sulphuric acid medium [33], no work to the best of our knowledge has been documented on the corrosion inhibition potentials of quinoline derivatives namely: namely 5-((X-1H-benzo[d]imidazol-1-yl)-methyl)quinolin-8-ol (X : -N(CH$_3$)$_2$and-NO$_2$) on hydrochloric acid solution. Recently a work was carried out in our laboratory on mild steel in 1 M HCl, with a new inhibitors entitled: 5-chloromethyl-8-hydroxyquinoline, and *N*-(8-hydroxyquinolin-5-yl)-methyl)-*N*-phenylacet-amide [34, 35].

The purpose of this paper is to synthesize and characterize new heterocyclic compound derivatives of 8-quinolinoland also to investigate their behavior as new inhibitors for the corrosion of mild steel in 1 M HCl solution using weight loss, electrochemical impedance spectroscopic (EIS) and potentiodynamic polarization methods (Tafel). The adsorption and inhibition efficiency of these inhibitors were investigated and the thermodynamic adsorption parameters in absence and presence of substituted quinolines were calculated. The effect of temperature on the corrosion behavior was also studied in the range from 298 K to328K.

2. Experimental details

2.1. Materials preparation

The chemical composition of steel is shown in Table 1. The specimen's surface was prepared by polishing with emery paper at different grit sizes (from 180 to 1200), rinsing with distilled water, degreasing in ethanol, and drying at hot air.

Corrosion tests were performed on mild steel which had the following chemical composition *(wt %)* balanced with (Fe).

Table 1*:* Chemical composition of the used mild steel

Material	Composition, % by wt											
	C	Si	Mn	Cr	Mo	Ni	Al	Cu	Co	V	W	Fe
mild steel	0.11	0.24	0.47	0.12	0.02	0.1	0.03	0.14	<0.0012	<0.003	0.06	Balance

The steels specimens used have a rectangular form 2.5 cm × 2.0 cm × 0.05 cm. The immersion time for weight loss was 6 h at 298 K. After immersion period, the specimens were cleaned according to ASTM G-81 and reweighed to 10^{-4} g for determining corrosion rate [21].

The aggressive solution of 1 M HCl was prepared by dilution of analytical grade 37 % HCl with distilled water. The molecular formula of the examined inhibitor is shown in **Table 2.**

Table 2: Names, chemical structures and abbreviations of the synthesized compounds.

Product Abbreviation	Chemical structure	Name of the compound
Q-N(CH₃)₂		5-((2-(4-dimethylamino)-phenyl-1H-benzo[d]imidazol-1-yl)-methyl)-quinolin-8-ol
Q-NO₂		5-((2-(4-nitrophenyl)-1H-benzo[d]imidazol-1-yl)methyl)-quinolin-8-ol

## 2.2. Synthesis and characterization of the inhibitors

2.2.1. General procedure for the preparation of **Q-NO₂** and **Q-N(CH₃)₂**

The mixture ofalkylebenzimidazole**5a, b** (1eq), 5-chloromethyl-8-hydroxyquinolinethe hydrochloride**2** (2 eq) in 50ml of tetrahydrofuran in the presence of triethylamine (2 eq) was stirred under reflux for 12 hours. When TLC (1:1 Hexane-acetone) indicated that the reaction was complete. The solvent was evaporated, the residue obtained was dissolved in chloroform (60 mL), and the resulting solution was washed twice with water. The organic layer was dried over anhydrous MgSO₄, filtered and the solvent was removed under reduced pressure to give a desired product. Recrystallization from ethanol gave **Q-NO₂**as a yellow solid and **Q-N(CH₃)₂**as a brown solid (schema 1).
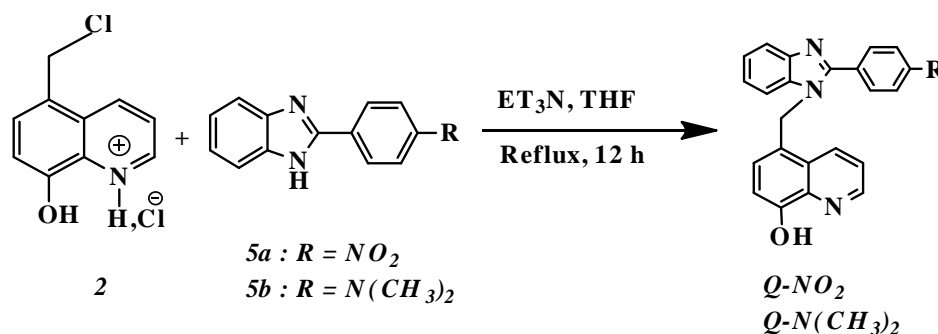
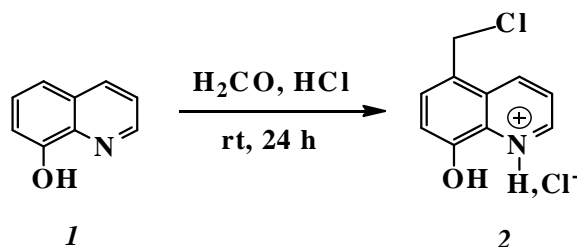**Scheme 1:** Synthetic route for the preparation of compounds **Q-NO₂** and **Q-N(CH₃)₂**

2.2.2. Synthesis of 2-alkylbezimidazoles **5a, b**

The synthesis of 2-(4-nitrophenyl)benzimidazole**5a**and 2-(4-dimetylaminophenyl)benzimidazole**5b**was realized according to the method described by Fortenberryet al. [22], which consists in the condensation of *o*-phenylenediamine**3** with the substituted benzaldehydes **4a,b** in the presence of ammonium hydrochloride in absolute ethanol. The mixture was stirred at room temperature for 24 h (Scheme 2).
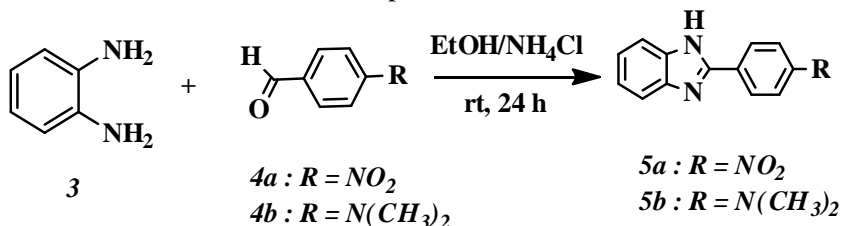
Scheme 2: Synthetic route for the preparation of 2-alkylbezimidazoles **5a,b**

2.2.3. Synthesis of 5-chloromethyl-8-hydroxyquinoline hydrochloride (2)

5-Chloromethyl-8-hydroxyquinoline hydrochloride **2**was prepared by adopting the method of Feng et al. [23], which consists in treating the mixture of 8-hydroxyquinoline **1**, formaldehyde (40 %) and concentrated hydrochloric acid (37 %) with dry hydrochloric acid gas for 24 hours (Scheme 3).

Scheme 3: Synthetic route for the preparation of 5-chloromethyl-8-hydroxyquinoline hydrochloride**2**

2.3. Corrosion weight loss tests

Weight loss experiments were done according to ASTM methods described previously [20, 21]. Tests were conducted in 1 M of HCl for 6 h at298 K. Gravimetric measurements were carried out in an electrolysis cell equipped with a thermostat-cooling condenser. The mild steel specimens used have a rectangular form 2.5 cm ×2.0 cm × 0.05 cm. After immersion period, the specimens were cleaned according to ASTM G-81 and reweighed to 10^{-4} g for determining corrosion rate [21].Duplicate experiments are performed in each case, and the mean value of the weight loss is reported. Weight loss allows us to calculate the mean corrosion rate as expressed in(mg $cm^{-2}h^{-1}$), either by chemical analysis of dissolved metal in solution or by gravimetric method measuring. The resulting quantity, corrosion rate (ω_{corr}) is thereby the fundamental measurement in corrosion. (ω_{corr}) can be determined weight of specimen before and after exposure in the aggressive solution applying the following equation 1:

$$\omega_{corr} = \frac{m_i - m_f}{S \times t} \qquad (1)$$

Where m_i, m_f, S and t denote initial weight, final weight, surface of specimen and immersion time, respectively.

The inhibition efficiency, η_ω%, is determined as follows:

$$\eta_\omega\left(\%\right) = \frac{\omega_{corr}^0 - \omega_{corr}}{\omega_{corr}^0} \times 100 \qquad (2)$$

Where ω^0_{corr} and ω_{corr} are the corrosion rates in the absence and presence of inhibitors, respectively.

2.4. Electrochemical cell
2.4.1. Potentiodynamic polarization measurement

For electrochemical measurements, the electrolysis cell was a borrosilcate glass (Pyrex®) cylinder closed by a cap with five apertures. Three of them were used for the electrode insertions. The working electrode was pressure-fitted into a polytetrafluoroethylene holder (PTFE) exposing only $1 cm^2$ of area to the solution. Platinum and saturated calomel were used as counter and reference electrode (SCE), respectively. All potentials were measured against the last electrode.

The potentiodynamic polarization curves were recorded by changing the electrode potential automatically from negative values to positive values versus E_{corr} using a Potentiostat/Galvanostat type PGZ 100, at a scan rate of 1 mV/s after 1 h of immersion time until reaching steady state. The test solution was thermostatically controlled at 298 K in air atmosphere without bubbling. To evaluate corrosion kinetic parameters, a fitting by Stern-Geary equation was used. To do so, the overall current density values i were considered as the sum of two contributions, anodic and cathodic current i_a and i_c, respectively. For the potential domain not too far the open circuit

potential, it may be considered that both processes followed the Tafel law [24]. Thus, it can be derived from equation (3):

$$i = i_a + i_c = i_{corr} \left\{ \exp\left[b_a \times (E - E_{corr}) \right] - \exp\left[b_c \times (E - E_{corr}) \right] \right\} \quad (3)$$

Where i_{corr} is the corrosion current density ($A\ cm^{-2}$), b_a and b_c are the Tafel constants of anodic and cathodic reactions (V^{-1}), respectively. These constants are linked to the Tafel slopes $\beta(V/dec)$ in usual logarithmic scale given by equation (4):

$$\beta = \frac{ln\,10}{b} = \frac{2.303}{b} \quad (4)$$

The corrosion parameters were then evaluated by means of nonlinear least square method by applying equation (3) using Origin software. However, for this calculation, the potential range applied was limited to ±0.100V around E_{corr}; else a significant systematic divergence was sometimes observed for both anodic and cathodic branches.

The corrosion inhibition efficiency is evaluated from the corrosion current densities values using the relationship (5):

$$\eta_{PP} = \frac{i_{corr}^0 - i_{corr}}{i_{corr}^0} \times 100 \quad (5)$$

The surface coverage values (θ) have been obtained from polarization curves for various concentrations of inhibitor using the following equation [25]:

$$\theta = 1 - \frac{i_{corr}}{i_{corr}^0} \quad (6)$$

Where i_{corr}^0 and i_{corr} are the corrosion current densities values without and with inhibitor, respectively.

2.4.2. Electrochemical impedance spectroscopy measurements (EIS)
The electrochemical measurements were carried out using Volta lab (Tacussel-Radiometer PGZ 100) potentiostat and controlled by Tacussel corrosion analysis software model (Voltamaster 4) at under static condition. The corrosion cell used had three electrodes. The reference electrode was a saturated calomel electrode (SCE). A platinum electrode was used as auxiliary electrode of surface area of 1 cm². The working electrode was mild steel. All potentials given in this study were referred to this reference electrode. The working electrode was immersed in test solution for 60 min to a establish steady state open circuit potential (E_{ocp}). After measuring the E_{ocp}, the electrochemical measurements were performed. All electrochemical tests have been performed in aerated solutions at 298 K. The EIS experiments were conducted in the frequency range with high limit of 100 KHz and different low limit 0.1 Hz at open circuit potential, with 10 points per decade, at the rest potential, after 60 min of acid immersion, by applying 10 mV ac voltage peak-to-peak. Nyquist plots were made from these experiments. The impedance data were analyzed and fitted with the simulation ZView 2.80, equivalent circuit software.

3. Results and discussion
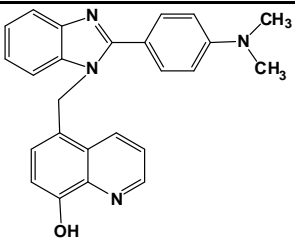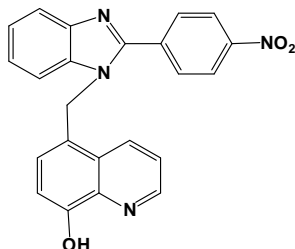### 3.1. Characterization of Q-N(CH₃)₂ and Q-NO₂
The synthesized compounds are characterized by ^{1}H and ^{13}C NMR spectroscopy. The results are given in Table 3.

3.2. Gravimetric measurements
The effect of different concentration of substituted quinoline compounds on the inhibition of mild steel corrosion in1 M HCl was studied using gravimetric method due to its simplicity and good reliability. The observed weight-loss values of triplicate measurements are highly reproducible giving standard deviations. The inhibition efficiency (η_ω%) and other parameters such as corrosion rate (ω_{corr}) and surface coverage (θ) at various concentration of the inhibitors are given in Table 4.Careful examination of the results showed that the inhibition efficiency increases with increasing the concentration. Maximum values of (inhibition efficiency) 93.1% for **Q-**

$N(CH_3)_2$ and 82.9% for$Q$-NO_2were obtained at 10^{-3}M. It has been reported that at lower concentrations, inhibitors preferably adsorb by flat orientation such that as the concentration increases, surface coverage and consequently inhibition efficiency increases. However, if the concentration of the inhibitor is increased beyond certain (optimum) value, the inhibitor molecules adsorb perpendicularly onto the metallic surface due to electrostatic repulsion between the molecules at higher concentration. Therefore, after the optimum concentration of the inhibitor, the inhibition performance does not change significantly.

Table 3: Yields and physicochemical characteristics of the compounds Q-$N(CH_3)_2$ and Q-NO_2

Product	Yield (%)	Mp (°C)	Spectral data
Q-N(CH₃)₂	80	143	^1H NMR (DMSO-d_6): δ_{ppm} =5.69 (S, 2H, CH₂), 5.33 (S, 1H, OH), 3.39 (S, 6H, (CH₃)₂) 7.03-7.53-7.58-7.61 (m, 8H, of benzimidazole), 7.06-7.57-7.60-8.46-8.87 (m, 5H, of quinoline). ^{13}C NMR (DMSO-d_6): δ_{ppm} = 53.60 (CH₂), 40.77 (CH₃) 153.40 (ArC-OH), 153.55 ((N=C(Ph)N), 119.29-122.58 (ArCH benzene of imidazole), 111.07-128.26 (ArC benzene of imidazole), 111.02-128.29 (ArCH of benzene), 121.72-153.55 (ArC of benzene), 117.56-127.57-133.01-148.39 (ArCH of quinoline),122.28-128.26-138.99 (ArC of quinoline).
Q-NO₂	65	123	^1H NMR (DMSO-d_6): δ_{ppm} =5.49 (S, 2H, CH₂), 5.45 (S, 1H, OH), 7.23-7.61-8.01-8.68 (m, 8H, of benzimidaz-ole), 8.70-8.66-7.66-7.26-6.94 (m, 5H, of quinoline). ^{13}C NMR (DMSO-d_6): δ_{ppm} = 69.53 (CH₂), 152.35 (ArC-OH), 153.91 ((N=C(Ph)N), 119.69-122.16 (ArCH benzene of imidazole), 139.17-139.24 (ArC benzene of imidazole), 124.63-127.74 (ArCH of benzene), 139.31-148.40 (ArC of benzene),111.07-122.12-126.90-132.69-148.24(ArCH of quinoline), 126.99-128.27-133.57 (ArC of quinoline).

The order of inhibition efficiencies in Table 4 is Q-$N(CH_3)_2$>Q-NO_2. The high inhibition efficiency of Q-$N(CH_3)_2$ compared to Q-NO_2 is due to the presence of electron donating -(CH₃) group in Q-$N(CH_3)_2$thereby enhances its ability to donate charges to the metal during the adsorption process.

Table 4: Weight loss data of mild steel in 1 M HCl without and with different concentrations of substituted quinoline derivatives at 298 K after 6 h of immersion

Inhibitor	[C](M)	ω_{corr} (mg cm^{-2} h^{-1})	η_ω (%)	θ
Q-N(CH₃)₂	0	38.93	—	—
	10^{-6}	9.20	76.4	0.764
	10^{-5}	6.01	84.6	0.846
	10^{-4}	3.89	90.1	0.901
	10^{-3}	2.67	**93.1**	0.931
Q-NO₂	0	38.93	—	—
	10^{-6}	32.70	32.7	0.327
	10^{-5}	19.20	50.7	0.507
	10^{-4}	18.01	53.7	0.537
	10^{-3}	6.67	**82.9**	0.829

3.3. Potentiodynamic polarization curves

Potentiodynamic polarization curves of mild steel in 1 M HCl without and with different concentrations of all substituted quinoline compounds are presented in Figures1 and 2. Their extrapolation parameters and inhibition efficiency values are given in Table 5. It can be shown that the quinoline addition hinders the acid attack on mild steel. In addition, an increase in their concentration gives a decrease in anodic and cathodic current densities indicating that the substituted quinoline compounds acts as mixed-type inhibitors. However, the inhibitor addition does not change the hydrogen evolution reaction mechanism such as indicated by the slight changes in the cathodic slopes (β_c) values. This indicates that hydrogen evolution is activation controlled [30, 31].
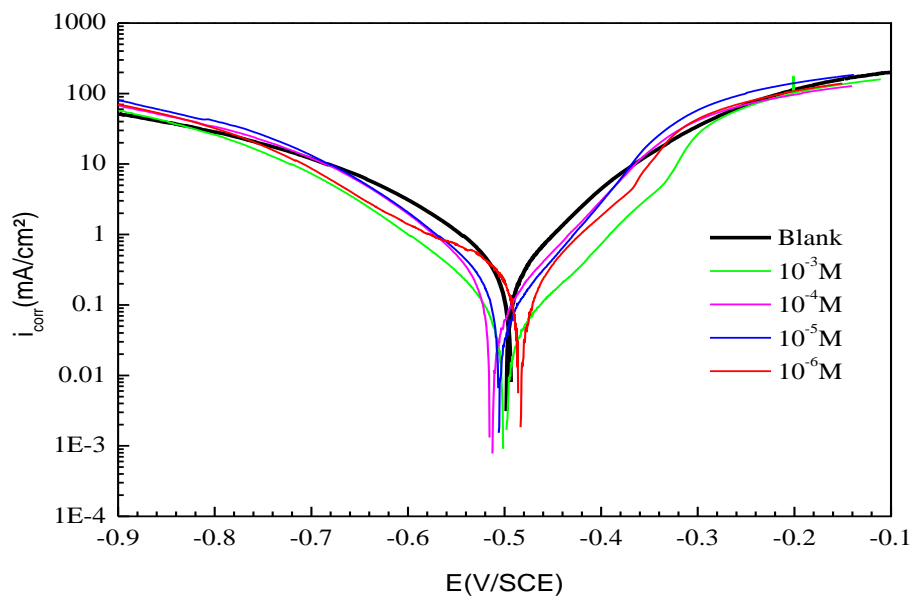

Figure1: Potentiodynamic polarization curves for mild steel in 1 M HCl in the absence and presence of various concentrations of *Q-NO₂*
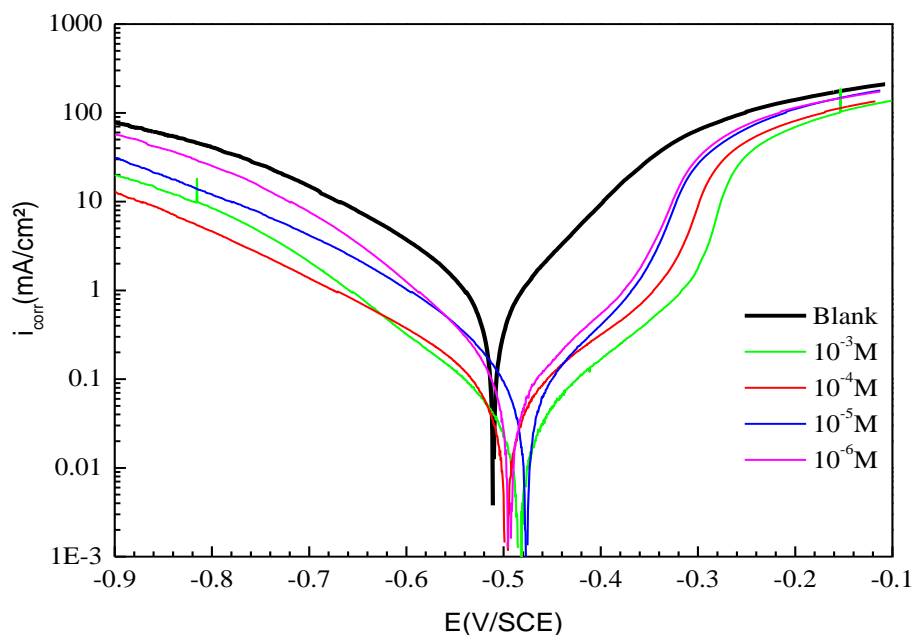

Figure2: Potentiodynamic polarization curves for mild steel in 1 M HCl in the absence and presence of various concentrations of *Q-N(CH₃)₂*

Table 5: Electrochemical parameters for mild steel in 1 M HCl at various concentrations of inhibitors at 298 K

Medium	[C] (M)	$-E_{corr}$ (mV vs. SCE)	i_{corr} ($\mu A\ cm^{-2}$)	Tafel slopes (mV dec^{-1})		η_{pp} (%)
				$-\beta_c$	β_a	
Blank solution	0	506	983	92	102	—
Q-N(CH₃)₂	10^{-6}	494	226	86	90	77.0
	10^{-5}	475	135	90	88	86.3
	10^{-4}	496	77	106	99	92.2
	10^{-3}	482	47	96	92	**95.2**
Q-NO₂	10^{-6}	484	644	153	78	34.5
	10^{-5}	513	490	85	66	50.2
	10^{-4}	504	450	87	62	54.3
	10^{-3}	499	179	84	73	**82.0**

The values of the slopes of the anodic Tafel lines, β_a, show a change with the addition of both inhibitors suggesting that the studied inhibitors was first adsorbed onto the metal surface and impeded by merely blocking the reaction sites of the metal surface without affecting the anodic reaction mechanism [36].

It is apparent also that the η_{PP} followed the order **Q-N(CH₃)₂ >Q-NO₂** such as found by the weight loss measurements. The results obtained by the potentiodynamic polarization curves confirm those obtained by weight loss measurements.

3.4. Electrochemical Impedance Spectroscopy (EIS)

Figures 4 and 5show typical Nyquist plots for the mild steel in 1 M HCl in absence and presence of different concentrations of **Q-N(CH₃)₂**and **Q-NO₂**. All of the impedance spectra mainly display depressed semicircles. The inhibition efficiencies η_{EIS}%, were calculated from Nyquist plots by the equation:

$$\eta_{EIS}(\%) = \left(\frac{R_{ct} - R_{ct}^{\circ}}{R_{ct}} \right) \times 100 \qquad (7)$$

Where R_{ct}° and R_{ct} are the charge transfer resistance of steel electrode in absence and in presence of inhibitor.

The impedance response of mild steel in 1 M HCl solution was significantly changed after the addition of both inhibitors and the impedance of the inhibited system increased with inhibitor concentration. Furthermore, at 10^{-3} M concentration of **Q-N(CH₃)₂**and **Q-NO₂** larger diameter semicircles were obtained than the other three lower concentrations of these compounds (Figures4 and 5). In the presence of these inhibitors, in the completely studied concentration interval, the electrochemical impedance spectra in complex plane depiction of Nyquist diagram show a depressed capacitive loop in the high frequency (HF) range and an inductive loop in the lower frequency (LF) range. The HF capacitive loop can be attributed to the charge transfer reaction and time constant of the electric double layer and to the surface non-homogeneity of interfacial origin, such as those found in adsorption processes on metal surface and the LF inductive loop may be attributed to the relaxation process obtained by adsorption of the species like Cl_{ads}^{-} and H_{ads}^{+} on working electrode surface [37-42].It may also be attributed to the adsorption of inhibitor on the electrode surface [43] or to the re-dissolution of the passivated surface at low frequencies [44]. In other words, the inductive behaviour at low frequency is probably due to the consequence of the layer stabilization by products of the corrosion reaction on the electrode surface (for example, [FeOH]ₐds and [FeH]ₐds) involving inhibitor molecules and their reactive products [45].

The LF inductive loop (10^{-4} M and 10^{-5} M) of **Q-NO₂**may be a consequence of the layer stabilization by-products of the corrosion reaction at the electrode involving inhibitor molecules and their reactive products [46]. The LF inductive loop was absent for 10^{-3} M and 10^{-6} M **Q-NO₂** concentration which may be attributed to the formation of a protective film causing hindrance in the dissolution process [47].

From *EIS* diagrams it was clear that the solution resistance R_s, charge-transfer resistance R_{ct}, constant phase element (CPE), and inductive elements of L and R_L were fitted (Figure3b) and for other inhibitor concentrations, (Figure3a) is a circuit generally used to model metal/acid interface [48]. Excellent fit with these two models were obtained for all experimental data. For the description of depressed semicircles with their centers below the real axis, a constant phase element (CPE) was used and expressed as [49]:

$$Z_{CPE} = \frac{1}{A(i\omega)^n} \quad (8)$$

where $A(\Omega^{-1}s^n\ cm^{-2})$ is the magnitude of the *CPE*, $\omega(rad\ s^{-1})$ is the sine wave modulation angular frequency, $i^2 = -1$ is the imaginary number and n is an empirical exponent which measures the deviation from the ideal capacitive behaviour [50,51]. Depending on the values of n, *CPE* can represent resistance ($n = 0$), capacitance ($n = 1$), inductance ($n = -1$) and Warburg impedance ($n = 0.5$) [52-54]. The values of double layer capacitance C_{dl} derived from the *CPE* and The relaxation time constant (τ) of charge-transfer process can be calculated using the equation (9) and (10) respectively [55].

$$C_{dl} = \sqrt[n]{A(R_{ct})^{1-n}} \quad (9)$$

$$\tau = C_{dl}R_{ct} \quad (10)$$

The impedance parameters, such as R_s, R_{ct}, A, n, L, R_L, C_{dl} and inhibition efficiency $\eta_Z(\%)$, obtained from fitting the *EIS* data using the equivalent circuit of Figure3, are calculated and listed in Table 6.
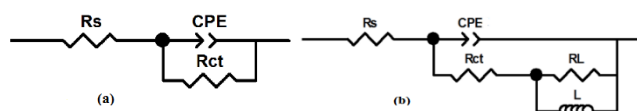

Figure 3:(a) Equivalent circuit used to fit the *EIS* data of mild steel in 1 M HCl without inductive loop. (b) Equivalent circuit used to fit the *EIS* data of mild steel in 1 M HCl with inductive loop.

As an example, The Nyquist and Bode plots of both experimental and simulated data of mild steel in 1.0 M HCl solution without and with 10^{-3} M and 10^{-5}M of *Q-NO₂* are shown in Figures 6, 7 and 8 respectively. Excellent fit with the models was obtained for all experimental data. It is clear that the impedance plots are in accordance with those calculated by the use of different equivalent circuit models.
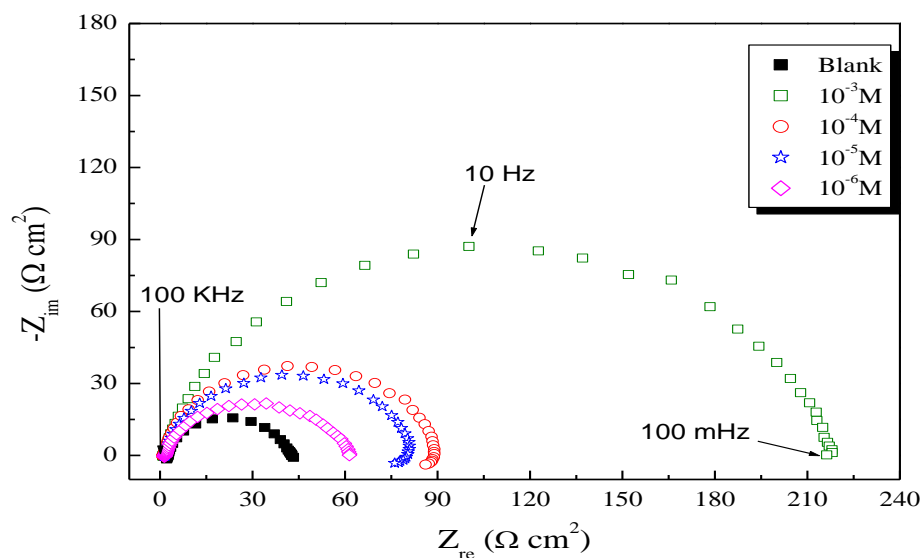

Figure 4: Nyquist plots for mild steel in 1 M HCl solution in the absence and presence of various concentrations of*Q-NO₂* at 298 K.
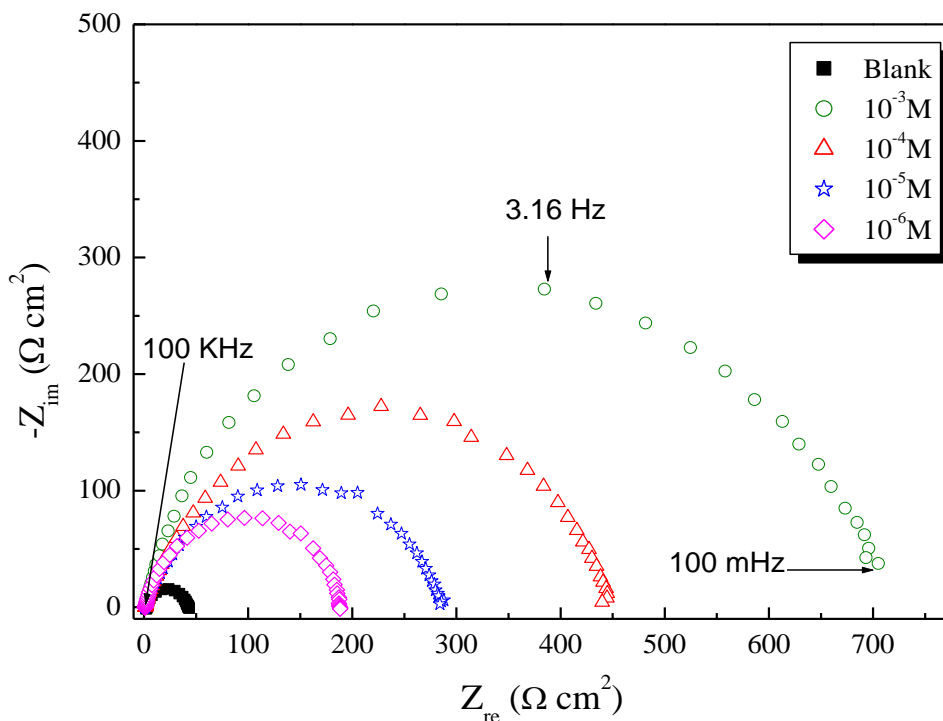
Figure 5: Nyquist plots for mild steel in 1 M HCl solution in the absence and presence of various concentrations of *Q-N(CH₃)₂* at 298 K.
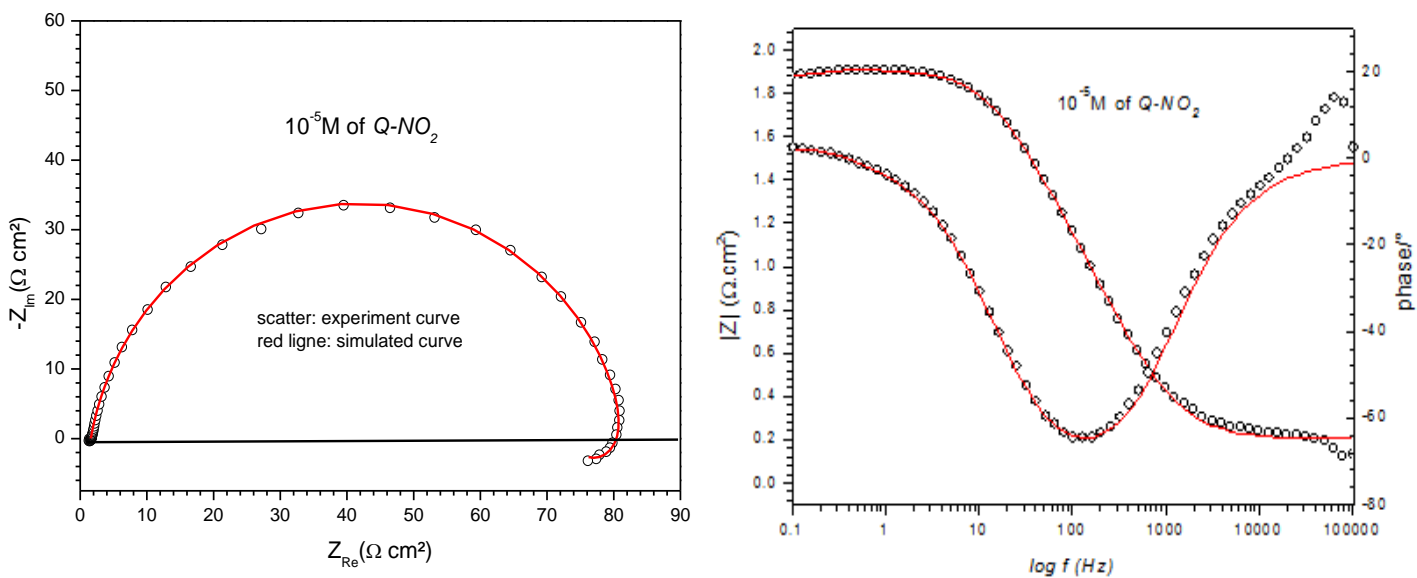

Figure 6: Nyquist and Bode plot for mild steel in 1 M HCl with 10^{-5} M of *Q-NO₂*

Inspection of the results in Table 6 indicated that R_{ct} value increased with the concentration of these inhibitors. In addition, the value of proportional factor *A* of *CPE* varies in the regular manner with BMNs concentration. The change in the values of R_{ct} and A can be related to the gradual removal of water molecules by *Q-NO₂* and *Q-N(CH₃)₂* molecules on the electrode surface and consequently leads to decrease in the number of active sites necessary for the corrosion reaction [56]. The increase in R_{ct} value is attributed to the formation of protective film

on the metal/ solution interface. The ongoing stability of *n* (in the range of 0.79-0.87) indicates the charge transfer controlled dissolution mechanism of mild steel in the absence and presence of **Q-NO₂**and**Q-N(CH₃)₂**.Moreover, the values of double-layer capacitance, C_{dl}, decreased with increasing **Q-NO₂**and**Q-N(CH₃)₂** concentrations.
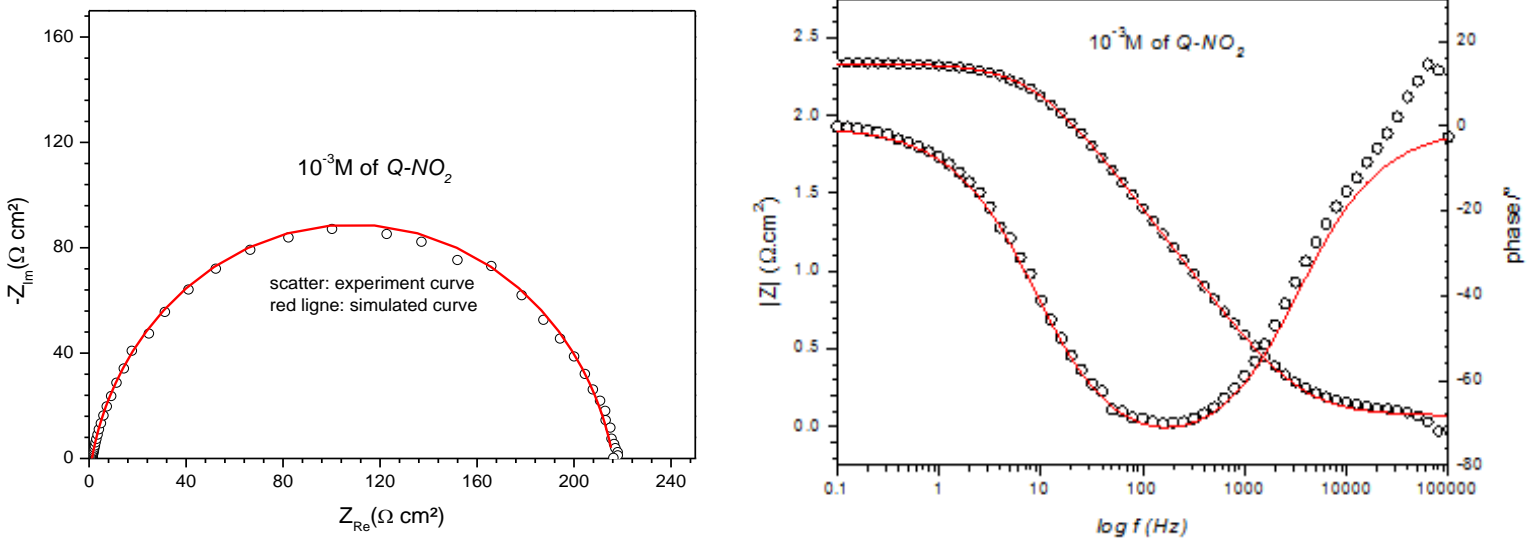

Figure 7: Nyquist and Bode plot for mild steel in 1 M HCl with 10^{-3} M of **Q-NO₂**
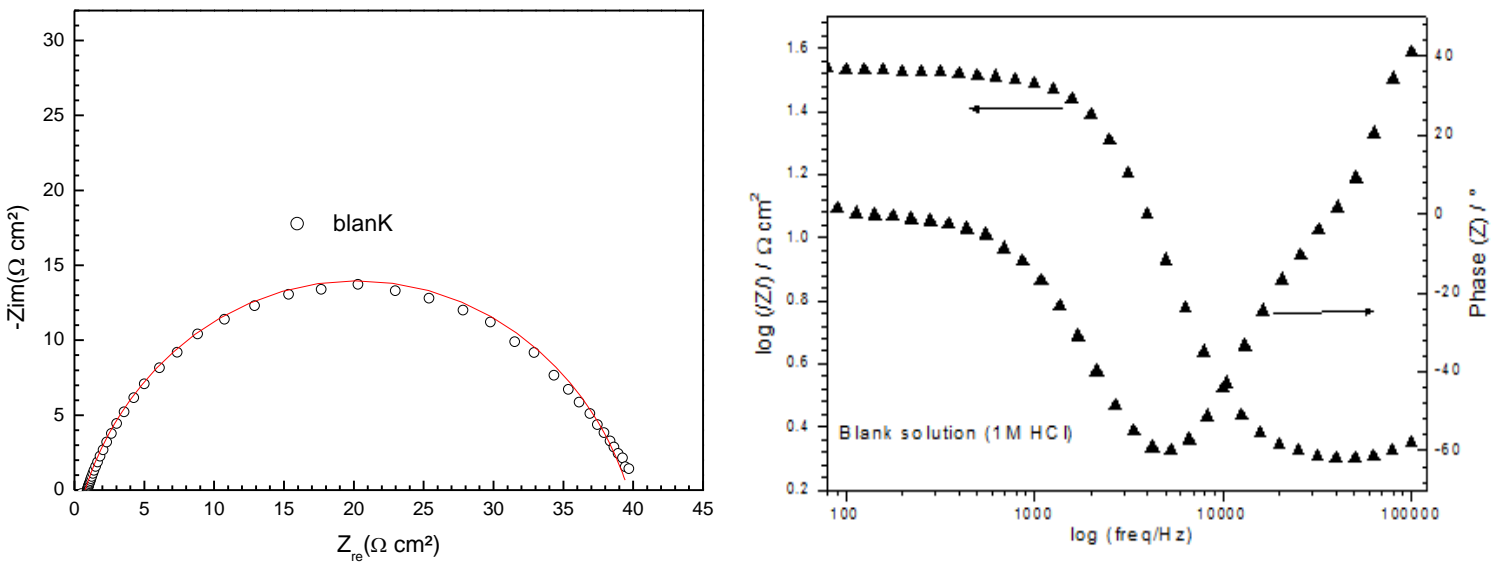

Figure 8: Nyquist and Bode plot for mild steel in 1 M HCl at 298 K

The decrease in C_{dl} is probably due to a decrease in local dielectric constant and/or an increase in the thickness of a electrical double layer at MS surface suggested that the removal of water molecules (with high dielectric constant) with inhibitor molecules (with low dielectric constant), therefore enhancing the resistance of the mild steel [57]. The thickness of this protective layer (d) is evaluated from the Helmholtz model, given by the following equation [58]:

$$C_{dl} = \frac{\varepsilon_0 \varepsilon}{e} S \qquad (11)$$

Whereε_0 is the permittivity of space, ε is the local dielectric constant, (e)is the film thickness and S is the surface area. Eq. (11) suggests that C_{dl} is inversely proportional to the thickness of protective layer d. So, the decrease in values of C_{dl} results in increase in values of d (Table 6).

Table 6: Electrochemical impedance parameters and the corresponding inhibition efficiencies for mild steel in 1 M HCl solution in the absence and presence of various concentrations of *Q-NO₂*and*Q-N(CH₃)₂* at 298 K

Inhibitor	[C] (M)	R_s ($\Omega.cm^2$)	R_{ct} ($\Omega.cm^2$)	CPE 10^4 A ($\Omega^{-1} S^n cm^2$)	n	C_{dl} ($\mu F\ cm^{-2}$)	R_L ($\Omega\ cm^2$)	L ($H\ cm^{-2}$)	τ_d (ms)	η_{EIS} (%)
Blank	00	5.22 ± 0.03	38.1 ± 0.4	4.3 ± 0.3	0.790±0.007	144.12	8.4 ± 0.4	1.83 ±0.31		—
Q-N(CH₃)₂	10^{-6}	1.17 ± 0.03	186.6± 0.7	1.6 ± 0.1	0.852±0.007	86.94	———	———	0.00547	79.6
	10^{-5}	1.11 ± 0.03	281.1± 0.9	1.4 ± 0.1	0.853±0.006	80.17	———	———	0.01622	86.5
	10^{-4}	1.37 ± 0.03	439.5± 1.1	1.2 ± 0.1	0.863±0.005	75.22	———	———	0.02254	91.3
	10^{-3}	1.32 ± 0.03	689.7± 1.2	1.1 ± 0.1	0.867±0.005	74.06	———	———	0.03306	**94.5**
Q-NO₂	10^{-6}	1.56 ± 0.02	58.2± 0.5	2.4 ± 0.2	0.824±0.008	96.40	———	———	0.05108	34.6
	10^{-5}	1.64 ± 0.02	72.0± 0.5	1.7 ± 0.1	0.850±0.007	78.16	7.8 ± 0.4	7.95 ± 0.62	0.00561	47.1
	10^{-4}	1.13 ± 0.02	75.6± 0.6	1.6 ± 0.1	0.857±0.008	76.59	11.7 ± 0.4	26.7 ± 0.91	0.00563	49.7
	10^{-3}	1.24 ± 0.02	212.7± 0.7	1.2 ± 0.1	0.858±0.006	65.39	———	———	0.00579	**82.1**

3.5. Effect of temperature

Temperature can modify the interaction between the steel electrode and the acidic media without and with substituted quinoline compounds inhibitor's. Polarization curves for mild steel in 1 M HCl in the absence and presence of 10^{-3} M of quinoline inhibitor's in the temperature range 298 K to 328 K are shown in Figures 9 to 11 presented the obtained potentiodynamic polarization curves and their corresponding data are presented in Table 7.
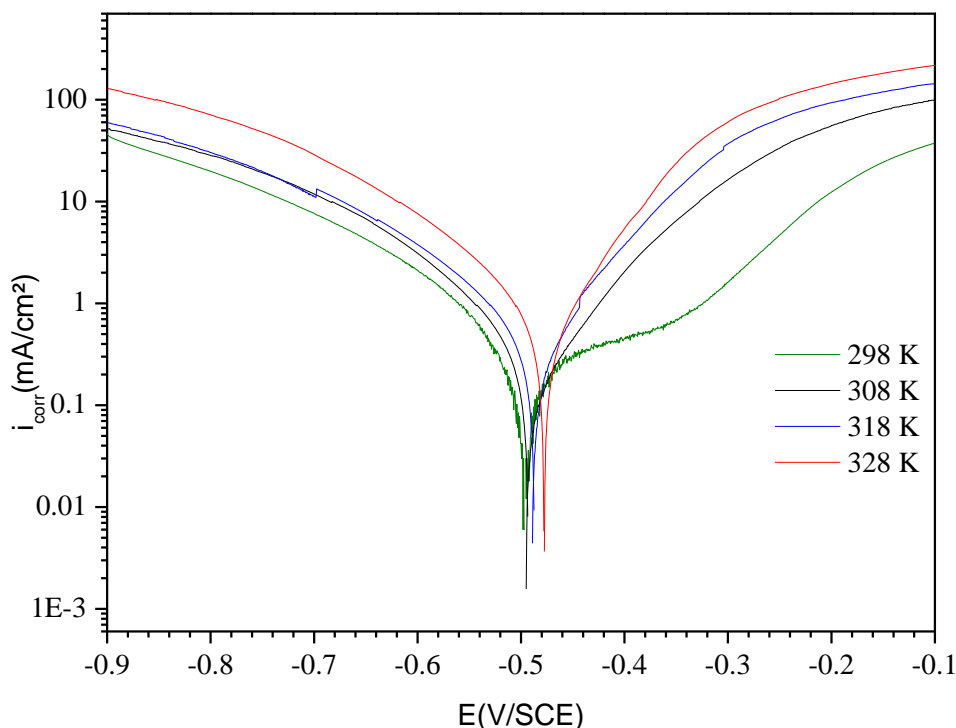

Figure 9: Potentiodynamic polarization curves for mild steel in 1 M HCl at different temperatures between 298 K and 328 K
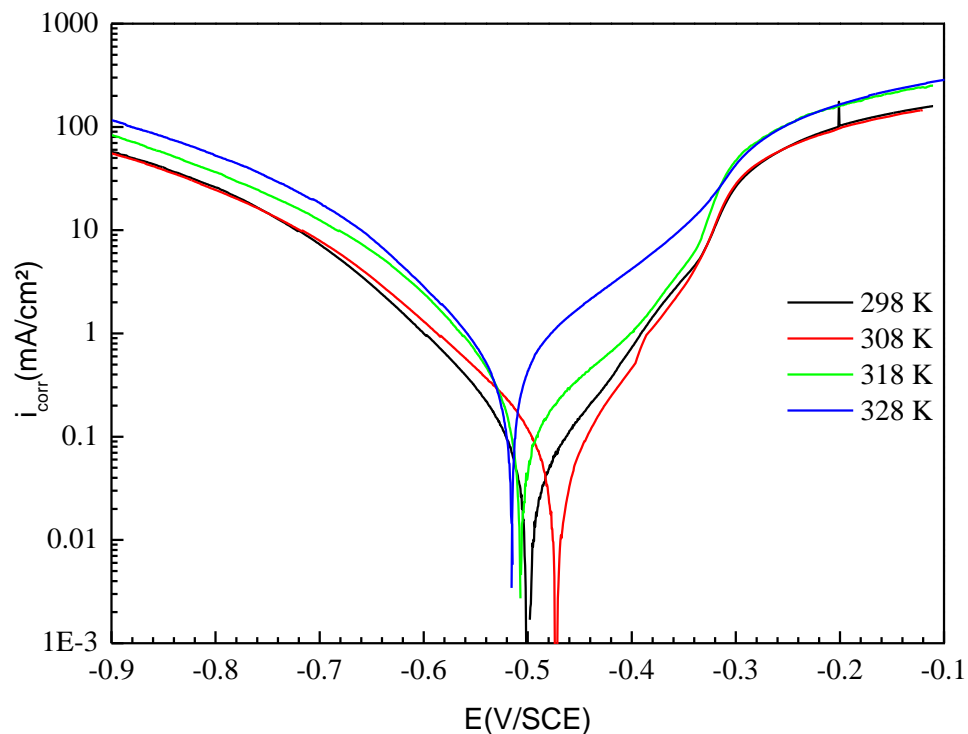
Figure 10: Potentiodynamic polarization curves for mild steel in 1 M HCl in the presence of 10^{-3} M of *Q-NO₂* at different temperatures between 298 K and 328 K
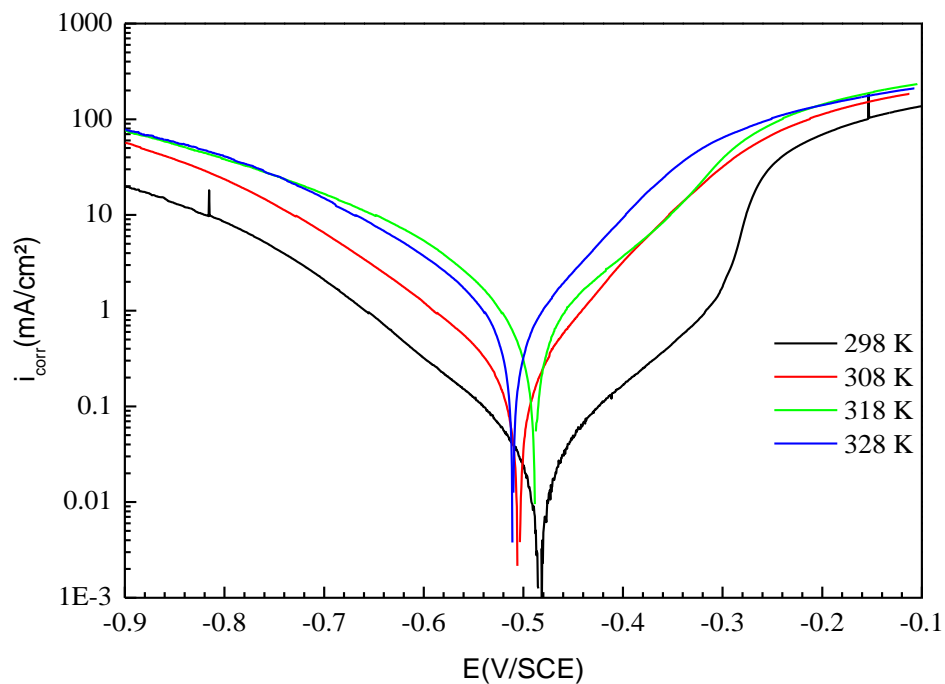

Figure 11: Potentiodynamic polarization curves for mild steel in 1 M HCl in the presence of 10^{-3} M of *Q-N(CH₃)₂* at different temperatures between 298 K and 328 K

Table 7: The influence of temperature on the electrochemical parameters for mild steel in 1 M HCl with 10^{-3} M of *Q-NO₂* and *Q-N(CH₃)₂*

Medium	T (K)	$-E_{corr}$ (mV$_{SCE}$)	i_{corr} (μA/cm²)	Tafel slopes (mV/dec)		η_{pp} (%)	θ
				$-\beta_c$	β_a		
Blank	298	498	983	92	104	—	—
	308	491	1200	184	112	—	—
	318	475	1450	171	124	—	—
	328	465	2200	161	118	—	—
Q-NO₂	298	499	179	84	102	82	0.82
	308	472	241	92.5	72	80	0.80
	318	505	302	82	68	79	0.79
	328	513	497	86	75	77	0.77
Q-N(CH₃)₂	298	482	47	96	92	95	0.95
	308	504	75	102	75	93	0.94
	318	487	145	93	102	90	0.90
	328	509	335	105	81	85	0.85

It is clear that all curves exhibit Tafel behaviour and show a little different effect in the anodic and cathodic branches. It is seen also that the inhibition efficiency decreased slightly with temperature.

3.5.1. Kinetic/Thermodynamics Considerations

The influence of temperature on the inhibition process of metal corrosion by an inhibitor is an important tool through which insight into the performance of inhibitor, activation processes, and the nature of adsorption of inhibitor on the corroding metal surface can be gained. Based on the effect of temperature, Rodovici [59] grouped inhibitors into three categories: (i) those whose inhibition efficiency decreases with increase in temperature. In this category, the apparent activation energy (E_a) in the inhibited solution is higher than that in the uninhibited solution; (ii) inhibitors whose inhibition efficiency is unaltered with variation in temperature. Here, the E_a in the inhibited and uninhibited solutions does not change with rise in temperature; (iii) those whose inhibition efficiency increases with increase in temperature. In this class, E_a for the inhibited system is lower than E_a of the uninhibited system. The apparent activation energy, E_a of the corrosion reaction was determined using Arrhenius plots. The Arrhenius equation could be written as:

$$i_{corr} = A\exp\left(\frac{-E_a}{RT}\right) \qquad (12)$$

Where i_{corr} is the corrosion current density, E_a is the apparent activation energy of the corrosion reaction and A is the Arrhenius pre-exponential factor.

The apparent activation energy of the corrosion reaction in presence and absence of the inhibitor could be determined by plotting *Ln (i_{corr})* with *1000/T* which gives a straight line (Figure 12) with a slope permitting the determination of E_a. Figure12 shows the Arrhenius plots in absence and presence of 10^{-3} M of quinoline inhibitor's. The corresponding values of E_a are given in Table 8 and indicate that values of E_a obtained in solutions containing *Q-NO₂* and *Q-N(CH₃)₂* are higher than those in the inhibitor-free acid solutions. The higher values of the apparent activation energy obtained in the presence of these compounds compared with those obtained in its absence, coupled with the observed decrease in inhibition efficiency with rise in temperature suggest that some of *Q-NO₂* and *Q-N(CH₃)₂* could be physisorbed on the steel surface [60].

An alternative formulation of Arrhenius equation (Eyring transition state equation) is [61]:

$$i_{corr} = \frac{RT}{Nh}\exp\left(\frac{\Delta S_a}{R}\right)\exp\left(\frac{\Delta H_a}{RT}\right) \quad (13)$$

Where h is Planck's constant, N is Avogadro's number, ΔS_a is the entropy of activation and ΔH_a is the enthalpy of activation. Figure 13 shows the variation of $Ln(i_{corr}/T)$ function $(1/T)$ as a straight line with as lope of $(-\Delta H_a/R)$ and the intersection with the y-axis is $[Ln(R/Nh) + (\Delta S_a/R)]$.
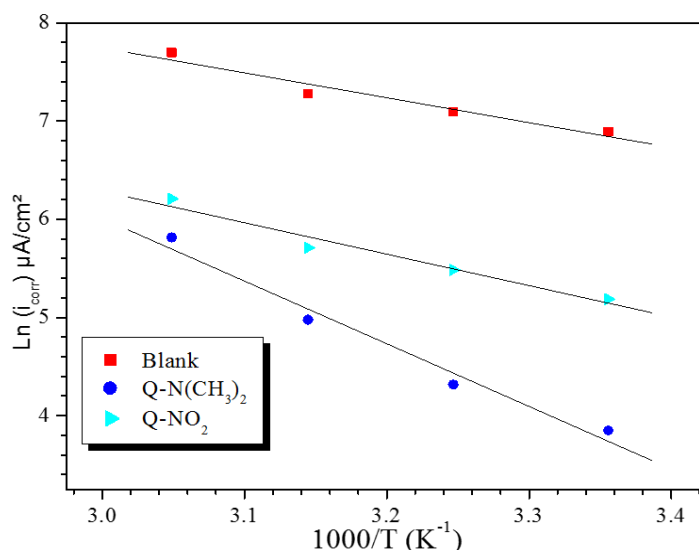

Figure 12: Arrhenius plots for mild steel corrosion in 1 M HCl in the absence and presence of **Q-NO₂** and **Q-N(CH₃)₂** at 10^{-3} M

Table 8: Activation parameters, E_a, ΔH_a and ΔS_a of the dissolution of mild steel in 1 M HCl in the absence and presence of **Q-NO₂** and **Q-N(CH₃)₂** at 10^{-3} M

Medium	E_a (KJ mol^{-1})	ΔH_a (KJ mol^{-1})	ΔS_a (J mol^{-1}K^{-1})
Blank	21.00	18.45	-126.00
Q-N(CH₃)₂	53.00	50.40	-44.60
Q-NO₂	26.60	24.00	-121.50

From these relationships, values of ΔS_a and ΔH_a can be determined. The activation parameters (ΔH_a and ΔS_a) which determined from the slopes of Arrhenius lines without and with inhibitors are summarized in Table8. It is seen that the ΔH_a value for dissolution reaction of mild steel in 1 M HCl in the presence of **Q-N(CH₃)₂** is higher than that in the presence **Q-NO₂** and the free solution. In addition, the ΔH_a values in the presence **Q-N(CH₃)₂** and **Q-NO₂** are higherthan that in their absence. However, the positive signs of ΔH_a values reveal the endothermic nature of the mild steel dissolution process suggesting that is difficult with inhibitors.

Entropy of activation provides some further insight into the mild steel adsorption process. This parameter assists with information regarding the extent of disorder of the adsorption/ desorption process between mild steel and inhibitor compounds. On comparing the values of entropy of activation (ΔS_a) listed in Table 8, it is clear that entropy of activation increases in presence of the studied inhibitors compared to free acid solution. Such variation is associated with the phenomenon of ordering and disordering of inhibitor molecules on the mild steel surface. The increased entropy of activation in the presence of inhibitor indicates that disorderness is increased on going from reactant to activated complex. The increase in values of entropy by the adsorption of inhibitor molecules on metal surface from the acid solution can be regarded as quasi-substitution between the inhibitor molecules in the aqueous phase and H_2O molecules on electrode surface. In such condition, the adsorption of inhibitor molecules is followed by desorption of H_2O molecules from the electrode surface. Thus increase in entropy of activation is attributed to solvent (H_2O) entropy.
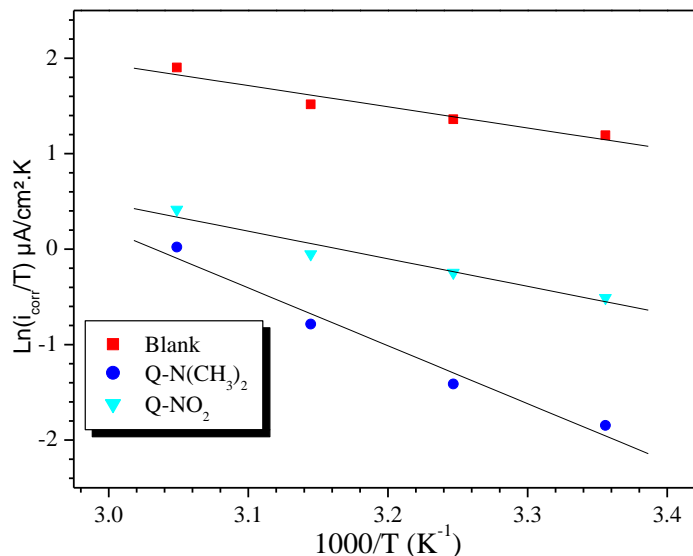
Figure 13: Transition state plot for mild steel corrosion in 1 M HCl in the absence and presence of **Q-NO₂** and **Q-N(CH₃)₂** at 10^{-3} M

3.6. Adsorption isotherm

Adsorption isotherm is very important in corrosion inhibition studies for the purpose of investigating the nature/mechanism and the rapidity/strength of the adsorption process. The adsorption isotherms provide structural as well as thermodynamic information of the adsorbed double layer. Several commonly used isotherms, namely Langmuir, Frumkin, and Temkin were tested among which the Langmuir isotherm showed the best fit with regression coefficient (R^2) values close to unity for all studied compounds. From this point of view, the current model has excellence in that it has only fitting parameter that quantifies the concentration dependence of adsorption. In our present investigation, attempts were made to fit to various isotherms which are expressed as [62, 63]:

Temkin isotherm: $$\exp(f\theta) = K_{ads}C \qquad (14)$$

Langmuir isotherm: $$\theta = K_{ads}C \qquad (15)$$

Frumkin isotherm: $$\frac{\theta}{1-\theta}\exp(-2f\theta) = K_{ads}C \quad (16)$$

Where K_{ads} is the binding constant of adsorption, C the inhibitor concentration, f the factor of energetic inhomogeneity, and θ the degree of surface coverage, was calculated using following formula:

$$\theta = \frac{\omega_{corr}^0 - \omega_{corr}}{\omega_{corr}^0} \qquad (17)$$

The Temkin, Frumkin, and Langmuir isotherms plots are given in Figure 14. Careful examination of the Figure 14 shows that among the tested isotherms, the Langmuir isotherm gave the best fit because in this case the values of R^2 are most close to unity for all inhibitors whereas for Frumkin and Temkin isotherms, the values of R^2 were much apart from unity. Further, although the values of R^2 in Langmuir adsorption isotherm were close to one, the considerable deviation of the slope from unity indicated that the Langmuir isotherm could not be strictly applied. The deviation of slope values from unity is attributed due to intermolecular interactions of adsorbed species which causes mutual repulsion or attraction [64, 65]. Moreover, the deviation of the slope could also be a result of the changes in the adsorption heat with increasing surface coverage which has not been considered during

derivation of Langmuir adsorption isotherm [66]. The value of equilibrium constant, K_{ads} was calculated from the intercept of the straight line of the Langmuir isotherm plots for all studied compounds at different temperatures.

The standard free energy of adsorption (ΔG_{ads}°), is related to the K_{ads} by the equation:

$$\Delta G_{ads}^{\circ} = -RTLn\left(55.55 K_{ads}\right) \qquad (18)$$

Where R is the universal gas constant, T the thermodynamic temperature and the value 55.55 in the above equation is the concentration of water in solution in mol/L.
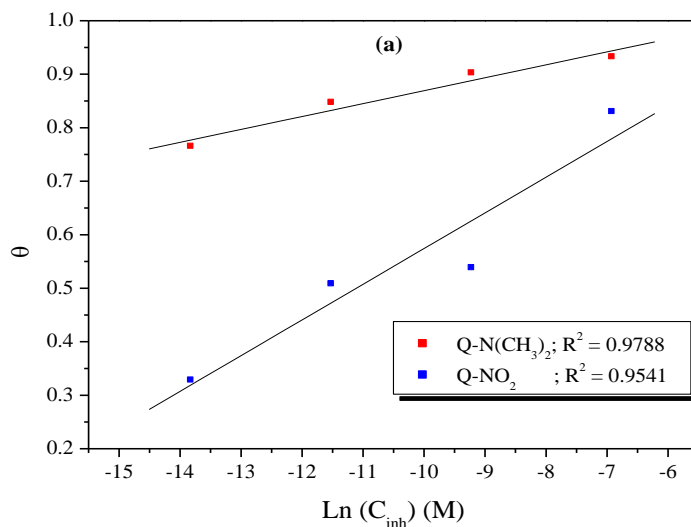

Figure 14(a): Temkin adsorption isotherm plots for the adsorption of *Q-N(CH₃)₂* and *Q-NO₂* on mild steel surface in 1 M HCl
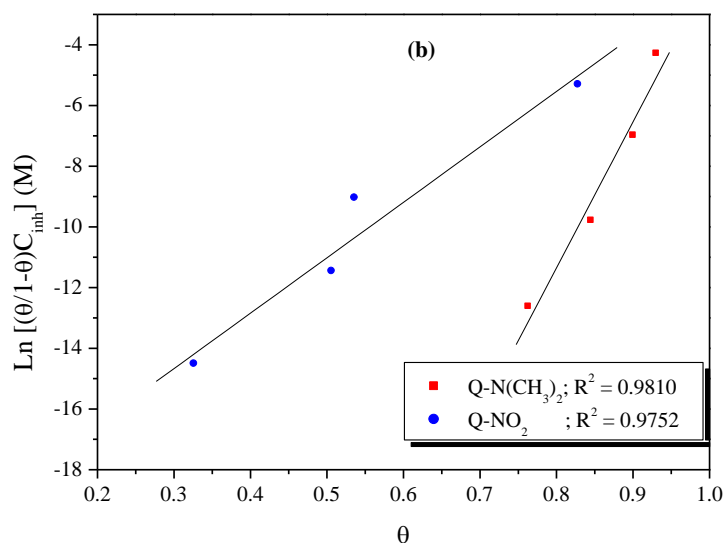

Figure 14(b): Frumkin adsorption isotherm plots for the adsorption of *Q-N(CH₃)₂* and *Q-NO₂* on mild steel surface in 1 M HCl
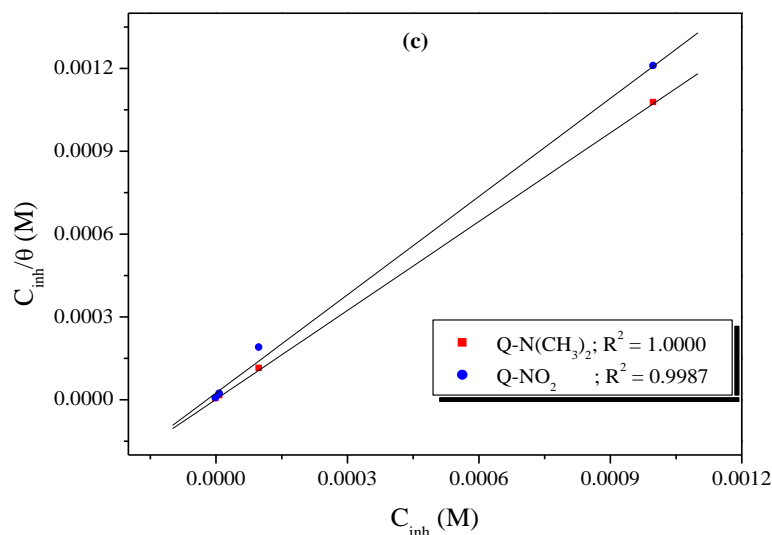
Figure 14(c): Langmuir adsorption isotherm plots for the adsorption of *Q-N(CH₃)₂*and*Q-NO₂*
on mild steel surface in 1 M HCl

The calculated values of K_{ads} and ΔG°_{ads} at each studied temperature in presence of optimum concentration of *Q-N(CH₃)₂*and *Q-NO₂* are given in Table 9. The high values of K_{ads} obtained for the studied compounds imply that the displacement of water molecules from the steel surface by the inhibitor molecules, and consequently the adsorption of the inhibitor molecules on the steel surface is a favorable process, and the compounds adsorb strongly on the steel surface.

However, it is observed that the slope (Table 9) for *Q-NO₂*remarkably deviated from unity required by an ideal Langmuir isotherm model. Langmuir equation had been derived under the assumption that adsorbed species do not interact with each other [67]. This assumption is not true as authors [68-70] have demonstrated that adsorbed inhibitor species are capable of interacting with each other on metal surface. For this reason, the values of *θ* were fitted into El-Awady kinetic/thermodynamic adsorption model which is a modification of the Langmuir isotherm and takes into consideration the omitted interaction parameter by Langmuir isotherm. Equation (19) [71] gives the description of the El-Awady kinetic/thermodynamic adsorption model.

$$Ln\left(\frac{\theta}{1-\theta}\right) = Ln\,K^{,} + y\,Ln\,C \quad (19)$$

Where *K'* is a constant, and y is the number of inhibitor molecules occupying one active site. A plot of *Ln (θ/1-θ)* versus *Ln C_{inh}* gives a straight line of slop y and intercept of *Ln K'*, as shown in Figure15. Equilibrium constant corresponding to adsorption isotherm is given by, $K_{ads} = K^{,1/y}$. Value of y > 1 implies the formation of multilayer of inhibitor on the surface of metal. Value of y < 1 mean a given inhibitor molecules will occupy more than one active site. All the adsorption parameters derived from Figures11c and 12 are listed in Table 9. The behavior of equilibrium constants obtained from Langmuir model was similar to the values which obtained by kinetic-thermodynamic model. The free energy of adsorption ΔG°_{ads} also can be calculated using the equation (18).

In general, the magnitude of ΔG°_{ads} is approximately -20 kJ/mol or less negative is assumed for existing electrostatic interactions between inhibitor and the charged metal surface (i.e., physisorption). Those ΔG°_{ads} around -40 kJ/mol or more negative are an indication of charge sharing or charge transferring from an organic species to the metal surface to form a coordinate type of metallic bond (i.e., chemisorption) [72].

It can be inferred from the range of values of ΔG_{ads}° in table 7 that the mode of adsorption of **Q-NO₂** involves competitive physisorption and chemisorption, while for the other inhibitor adsorb mainly via charge sharing (chemisorption). The trend of the values of K_{ads} and ΔG_{ads}° is such that **Q-NO₂>Q-N(CH₃)₂**, which is the same as the relative order of the %IE.
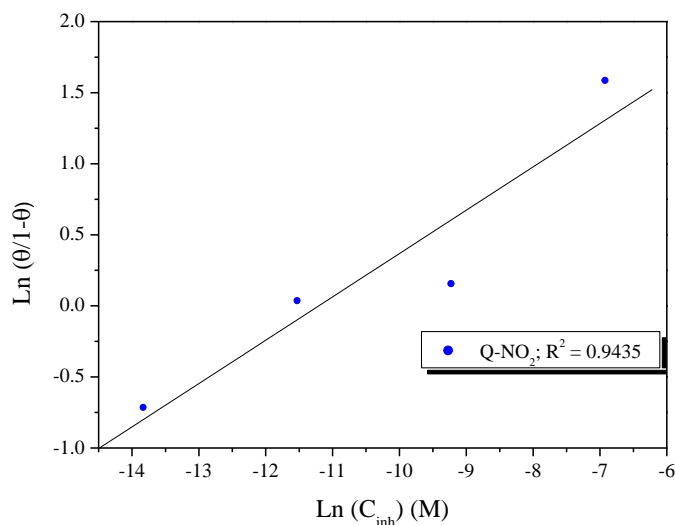

Figure 15: El-Awadyet al. Kinetic/thermodynamic isotherm for **Q-NO₂** in 1 M HCl at 298 K

Table 9. Adsorption parameters from Langmuir and El-Awadyet al. Kinetic/thermodynamic isotherms for mild steel in 1 M HCl in the absence and presence of different concentrations of **Q-N(CH₃)₂** and **Q-NO₂** at 298 K.

Isotherm's	Langmuir				El-Awady et al.			
Inhibitor	K_{ads} (M⁻¹)	ΔG_{ads}° (kJ/mol)	Slopes	R^2	K_{ads} (M⁻¹)	ΔG_{ads}° (kJ/mol)	1/y	R^2
Q-N(CH₃)₂	619417.50	-43.00	1.07	1.0000	——	——	—	——
Q-NO₂	40971.01	-36.27	1.19	0.9987	73903.48	-37.73	3.28	0.9435

Conclusion

All the examined substituted quinoline compounds are effective corrosion inhibitors for mild steel in 1M HCl solution. The inhibition efficiency increased with increasing concentration but decrease with temperature of the synthesized inhibitors and the order of inhibition efficiency decreased as follows: **Q-N(CH₃)₂>Q-NO₂**.These compounds react as mixed type inhibitors. The results of *EIS* indicate that the values of C_{dl} tend to decrease and both R_{ct} and η% tends to increase with increasing the inhibitors concentrations. This result can be attributed to an increase of the thickness of the protective film formed on the mild steel surface. These inhibitors were found to obey Langmuir adsorption isotherm and thermodynamic- kinetic model of El-Awady from the fit of experimental data. The results obtained from weight loss, impedance and polarization studies are in a good agreement.

References

1. El Kacimi Y., Touir R., M. Galai M., R. Belakhmima A., Zarrouk A., Alaoui M., Harcharras M., El Kafssaoui H., EbnTouhami M., *J. Mater. Environ. Sci*., 7 (2016) 371.
2. Galai M., Rbaa M., El Kacimi Y., Ouakki M., Dkhirech N., Touir R., Lakhrissi B., Ebn Touhami M., *Anal. Bioanal. Electrochem*., 9(2017) 80.
3. Abbouda Y., Abourriche A., Saffaj T., Berrada M., Charrouf M., Bennamara A., Al Himidi N., Hannache H., *Mater. Chem. Phys.*, 105 (2007) 1.
4. James A.O., Oforka N.C., Abiola K., *Int. J. Electrochem. Sci*., 2 (2007) 284.
5. Ebenso E.E., *Niger. J. Chem. Res*., 6 (2001) 12.
6. Ekpe U.J., Okafor P.C., Ebenso E.E., Offiong O.E., Ita B.I., *Bull. Electrochem*.,17 (2001) 135.
7. Elkacimi Y., Achnin M., Aouine Y., EbnTouhami M., Alami A., Touir R., Sfaira M., Chebabe D., Elachqar A., Hammouti B., *Portugaliae Electrochimica Acta*, 30 (2012) 53.
8. Dahmani K., Galai M., Elhasnaoui A., Temmar B., El Hessni A., Cherkaoui M., *Der Pharma Chemica*, 7 (2015) 566.
9. Esmaeel Naderi A., Jafari H., Ehteshamzadeh M., Hosseini M. G., *Mater.Chem.Phys.*, 115 (2009) 852.
10. Bentiss F., Lagrenee M., Traisnel M., Hornez J. C., *Corros. Sci*., 41 (1999) 789.
11. Galai M., El Gouri M., Dagdag O., El Kacimi Y., Elharfi A., Ebn Touhami M., *J. Mater. Environ. Sci*., 7(2016)1562.
12. Ehteshamzade M., Shahrabi T., Hosseini M. G., *Appl. Surf. Sci*., 252 (2006) 2949.
13. Galai M., El Faydy M., El Kacimi Y., Dahmani K., Alaoui K., Touir R., Lakhrissi B., EbnTouhami M., *Portugaliae Electrochimica Acta*., 35 (2017)233.
14. Abd El-Maksoud S.A., *Appl. Surf. Sci*., 206 (2003) 129.
15. Hassan H.H., Abdelghani E., Amina M.A., *Electrochim. Acta*, 52 (2007) 6359.
16. Kertit S., Hammouti B., *Appl. Surf. Sci*., 161 (1996) 59.
17. Gomma G.K., *Mater. Chem. Phys*., 55 (1998) 241.
18. Chetouani A., Hammouti B., Benhadda T., Daoudi M., *Appl. Surf. Sci*., 249 (2005) 375.
19. El Kacimi Y., Azaroual M.A., Touir R., Galai M., Alaoui K., Sfaira M., EbnTouhami M., Kaya S., *Euro-Mediterr J Environ Integr.,* 2 (2017) 1.
20. Chetouani A., Aounti A., Hammouti B., Benchat N., Benhadda T., Kertit S., *Corros. Sci*., 45 (2003) 1675.
21. Wahdan M.H., *Mater. Chem. Phys*., 49 (1997) 135.
22. Fortenberry B., Nammalwar B., Bunce R.A., *Organic Preparations and Procedures International*, 45 (1) (2013) 57.
23. Feng L., Wang X., Chen Z., Spectrochimica Acta Part A: *Molecular and Biomolecular Spectroscopy*, 71 (2) (2008) 312.
24. Obot I.B., Obi-Egbedi N.O., *Corros. Sci*., 52 (2010) 282.
25. Obot I.B., Obi-Egbedi N.O., *Corros. Sci*., 52 (2010) 923.
26. Obot I.B.,. Obi-Egbedi N.O, *Mater. Chem. Phys*., 122 (2010) 325.
27. Watson A.A., Fleet G.W.J., Asano N., Molyneux R.J., Nugh R.J., *Phytochemistry*, 56 (2001) 265.
28. Atwell G.J., Baguley B.C., Denny W.A., *J. Med. Chem*., 32 (1989) 396.
29. Xia Y., Yang Z.Y., Xia P., Bastow K.F., Tachibani Y., Kuo S.C., Hamel E., Hackl T., Lee K.H., *J. Med. Chem*., 41 (1998) 1155.
30. El Faydy M., Dahaief N., Rbaa M., Ounine K., Lakhrissi B*., J. Mater. Environ. Sci*., 7 (1) (2016) 356.
31. Peters W., Chemotherapy and Drug Resistance in Malaria, *Academic Press London*, New York(1970).
32. Sato M., Motomura T., Aramaki H., *J. Med. Chem*., 49(5) (2006) 1506.
33. Singh M., Bhattamishra A.K., *J. Mettalurgy Mater. Sci*., 49 (1) (2007) 51.
34. Elfaydy M., Lgaz H., Salghi R., Larouj M., Jodeh S., Rbaa M., Lakhrissi B., *J. Mater. Environ. Sci.*, 7 (9) (2016) 3193.
35. El Faydy M., Galai M., El Assyry A., Touir R., Ebn Touhami M., Benali B., Lakhrissi B., Zarrouk A., *J. Mater. Environ. Sci*., 7 (4) (2016) 1406.
36. Dahmani K., Galai M., Cherkaoui M., El hasnaoui A., El Hessni A., J. *Mater. Environ. Sci*., 8 (2017) 1676.

37. Amin M.A., Abd El-Rehim S.S., El-Sherbini E. E.F., Bayyomi R.S., *Electrochim. Acta*, 52 (11) (2007) 3588.
38. Lenderink H.J.W., Linden M.V.D., De Wit J.H.W., *Electrochim. Acta*, 38 (14) (1993) 1989.
39. Amin M.A., Khaled K.F.,Mohsen Q., Arida H.A., *Corros. Sci.*, 52 (5) (2010) 1684.
40. Kedam M., Mattos O.R., Takenouti H., *J. Electrochem. Soc.*, 128 (2) (1981) 257.
41. Veloz M.A., Gonzalez I., *Electrochim. Acta*, 48 (2) (2002) 135.
42. Lebrini M., Robert F., Lecante A., Roos C., *Corros. Sci.*, 53 (2) (2011) 687.
43. Alaoui K., El Kacimi Y., Galai M., Touir R., Dahmani K., Harfi A., Ebn Touhami M., *J. Mater. Environ. Sci*., 7 (7) (2016) 2389-2403.
44. Ghazoui A., Benchat N., El-Hajjaji F., Taleb M., Rais Z., Saddik R., Elaatiaoui A., Hammouti B., *Journal of Alloys and Compounds*, 693 (2017) 510-517
45. Kelly E.J., *J. Electrochem. Soc.*, 112 (1965) 125.
46. Lin Y., Singh A., Ebenso E.E., Wu Y., Zhu C., Zhu H., Tai J.*, Inst. Chem. Eng*., 46(2015) 214.
47. Tazouti A., Galai M., Touir R., Ebn Touhami M., Zarrouk A., Ramli Y., Saraçoğlu M., Kaya S., Kandemirli F., Kaya C., *J. Mol. Liq*., 221 (2016)815.
48. Tao Z., Zhang S., Li W., Hou B., *Ind. Eng. Chem. Res*., 50 (2011) 6082.
49. M'hanni N., Galai M., Anik T., Ebn Touhami M., Rifi E.H., Asfari Z., Touir R., *Surface &Coatings Technology*., 310 (2017) 8.
50. Lopez D.A., Simison S.N., de Sanchez S.R., *Electrochim. Acta*., 48 (7) (2003) 845.
51. Stoynov Z.B., Grafov B.M., Savova-Stoynova B., Elkin V.V., Electrochemical Impedance. Nauka. Moscow,(1991).
52. Musa A.Y., Kadhum A.A.H., Mohamad A.B., Takriff M.S., *Corros. Sci.*, 52 (10) (2010) 3331.
53. Labjar N., Lebrini M., Bentiss F., Chihib N., El Hajjaji S., Jama C., *Mater. Chem. Phys.*, 119 (1-2) (2010) 330.
54. Zheng X., Zhang S., Li W., Yin L., He J., Wua J., *Corros. Sci.*, 80 (2014) 383.
55. Bentiss F., Outirite M., Traisnel M., Vezin H., Lagrenée M., Hammouti B., Al-Deyab S.S., Jama C., *Int. J. Electrochem. Sci*., 7 (2012) 1699.
56.Bentiss F., Lebrini M., Lagrenee M., Traisnel M., Elfarouk A., Vezin H., *Electrochim. Acta*, 52 (2007) 6865.
57. Alaoui K., El Kacimi Y., Galai M., Dahmani K., Touir R., El Harfi A., Ebn Touhami M., *Anal. Bioanal. Electrochem*., 8, (2016)830.
58. Hassan H.H., *Electrochim. Acta*, 51 (2006) 5966.
59. Radovici O., Proceedings of the 2nd European Symposium on Corrosion Inhibition (1965); Ferrara, 178.
60. Benabida A., Galai M., Cherkaoui M., Dagdag O., *Anal. Bioanal. Electrochem*.,8 (2016) 962-976
61. Behpour M., Ghoreishi S.M., Mohammadi N., Soltani N., Salavati-Niasari M., *Corros. Sci*., 52 (2010) 4046.
62. Yadav D.K., Maiti B., Quraishi M.A., *Corros. Sci*., 52 (2010) 3586.
63. Obi-Egbedi N.O., Essien K.E., Obot I.B., *J. Comput. Method Mol. Des*., 1(1) (2011) 26.
64. Obot I.B., Obi-Egbedi N.O.,Umoren S.A., *Int. J. Electrochem. Sci*., 4 (2009) 863.
65. El Hezzat M., Zarrok H., Benzekri Z., El Assyry A., Boukhris S., Souizi A., Galai M., Touir R., Ebn Touhami M., Oudda H., Zarrouk A., *Der Pharma. Lettre*, 7(2015)239.
66. Oguzie E.E., Okolue B.N., Ebenso E.E., Onuoha G.N., Onuchukwu A.I., *Mater. Chem. Phys.*, 87 (2004) 394.
67. Solomon M.M., Umoren S.A., Udosoro I.I., Udoh A.P., *Corros. Sci*., 52 (2010) 1317.
68. Solomon M.M., Umoren S.A., *Measurement*, 76 (2015) 104.
69. El-Awady A.A., Abd-El-Nabey B.A., Aziz S.G.,*J. Electrochem. Soc*., 139 (1992) 2149.
70. Abd El Rehim S.S., Ibrahim A.M., Khalid K.F., *Mater. Chem. Phys*., 70 (2001) 268.
71. Ben Hmamou D., Salghi R., Zarrouk A., Zarrok H., Hammouti B., Al-Deyab S.S., El Assyry A., Benchat N., Bouachrine M., *Int. J. Electrochem. Sci*.,8(2013) 11526.
72. Serrar H., Belayachi M., Zarrouk A., Oudda H., Ebn Touhami M., El Hezzat M., Boukhris S., Souizi A., Galai M., *Der Pharma.Lettre*, 5 (2013)173.

(2017) ; http://www.jmaterenvironsci.com